

A Self-Diagnostic Adhesive for Bonded Joints in Aircraft Structures

Yitao Zhuang, Fotis Kopsaftopoulos, Fu-Kuo Chang
Aeronautics & Astronautics Department, Stanford University
496 Lomita Mall, Durand Building
Stanford, CA, 94305

ABSTRACT

Bondline integrity is still one of the most critical concerns in the design of aircraft structures up to date. Due to the lack of confidence on the integrity of the bondline both during fabrication and service, the industry standards and regulations require assembling the composites using the inefficient “Black-aluminum” approach, i.e. drill holes and use fasteners. Furthermore, current state-of-the-art non-destructive evaluation (NDE) and structural health monitoring (SHM) techniques are incapable of offering mature solutions on the issue of bondline integrity monitoring. Therefore, the objective of this work is to investigate the feasibility to embed piezoelectric sensors into the adhesively bonded joints in order to detect bondlines degradation.

The proposed method makes use of an electromechanical-impedance (EMI) based method, which is a rapidly evolving approach within the SHM family. This approach is based on the use of (i) micro-sensors integrated into adhesive leaving a minimal footprint on the material, (ii) numerical and analytical modeling of the EMI spectrum of the adhesive bondline, (iii) electromechanical impedance based diagnostic algorithms for monitoring the bondline integrity, and (iv) the experimental assessment via prototype adhesively bonded structures in static (varying loads) environment. The obtained results demonstrate the potential of the approach in providing increased confidence on the use of bonded joints for aerospace structures

1. INTRODUCTION

Bondline integrity monitoring is still one of the most critical concerns in the design of aircraft and spacecraft structures up to date. Although adhesively bonded joints have demonstrated superior properties over mechanically fastened joints, current standards still require fasteners even with adhesive because of a lack of confidence on the integrity of the bondline in fabrication and during service. This reduces the benefits of bonding. There are two major types of defects in bondlines, gross defects and adhesive defects [1]. Debonds between adhesive/adherend and delaminations on substrates, which fit into first category, can be detected via NDE methods like C-Scan or ultrasonic reflection [2-5]. Those methods have been proven to be effective to a certain extent. However, specimen preparation takes a long time in all of these methods. Recent work in structural health monitoring, by J.B. Ihn and F.K. Chang [6-8], has demonstrated the ability to identify debonds in real-time, using built-in piezoelectric discs to generate ultrasonic waves.

An adhesive defect is seen as traction-free contacted surfaces, which show reduced bond strength and are difficult or impossible to detect using conventional NDE [5]. Kissing bonds are one of the major adhesive defects and possess little residual tensile or shear strength. Many factors may lead to kissing bonds, including surface contaminates, adhesive chemistry, inappropriate curing stress, residual stress, moisture ingress, etc. As a result, kissing bonds can appear in a local fashion and the only way to detect them is to measure the local adhesive during fabrication and in service to

CAMX - The Composites and Advanced Materials Expo
October 27-29 2015, Dallas, TX, USA

track its degradation [5, 9-17]. Kissing bonds are the most critical and challenging defect to be detected in bonded joints and significantly influences the confidence of bondline integrity after the joints are placed in service.

Embedding micro/nano sensors inside the adhesive layer has the potential to be an effective solution to this challenge. Upon initial inspection, this approach may not seem feasible because adding new materials inside adhesive will increase the risk of contamination and introducing new defects. However, industry has begun to use adhesive films with fiber scrims inside, to ease handling and improve quality control. Relevant standard have been developed for this practice like BMS 5-121 TY.1. This indicates that this approach is feasible if the standards can be met by shrinking the sensors down to the size of typical fibers and making them out of the same materials as current scrims so that the adhesive will have the same mechanical performance as well as the capability to monitor its own integrity degradation level.

2. EXPERIMENTATION

2.1 Characterization of Carbon Fiber Reinforced Panels with Simulated Kissing Bond

Static shear test was conducted on the single shear sample fabricated by Boeing to understand the effect of kissing bond on the bondlines' performance. The sample consisted two carbon fiber reinforce plastic panels (152.4 mm x 457.2 mm or 6 inch x 18 inch) bonded together with Hysol EA9696 adhesive film. One panel was 16 plies stack (0-90 fabrics on the first and last layer, and [-45/90/45/-45/0/45/0]_s is the middles) and the other was 20 plies (0-90 fabrics on the first and last layer, and [-45/90/45/0/-45/0/0/45/0]_s is the middles). The material system was not labeled. With its own receipt on surface preparation, Boeing was able to tune the bondline strength into different levels. On the sample provided by Boeing, three levels of strength were achieved on different regions as weak (strength predicted to be 8.62 MPa or 1250 psi), medium (17.24 MPa or 2500 psi) and nominal (27.58 MPa or 4000 psi) bond

The bonded panels were cut into 25.4 mm x 152.7 mm (1 inch x 6 inch) strips with trenches of 2.54 mm (0.1 inch) width following ASTM D5868 (Standard Test Method for Lap Shear Adhesion for Fiber Reinforced Plastic (FRP) Bonding) in order to evaluate the bondline strength in static shear load test.

The test result of load-displacement and the failure patterns is shown in Figure 1. The strength of the weak bond was measured at $13.58 \pm 7\%$ MPa ($1970 \pm 7\%$ psi), the medium bond was $20.89 \pm 2\%$ MPa ($3030 \pm 2\%$ psi) and the nominal bond was $28.68 \pm 4\%$ MPa ($4160 \pm 4\%$ psi). The failure patterns of weak and medium bond were adhesive failure while the pattern of nominal bond was cohesive failure. The kissing bond (weak) resulted in a 50% loss of strength compared to the nominal bond and the failure pattern indicated that the weak adhesion between adhesive and substrate material caused the decrease of the bondline strength. The load-displacement curves of different strength levels overlapped, which implied that the existence of kissing bonds had very limited effect on the global stiffness of the bonded structure.

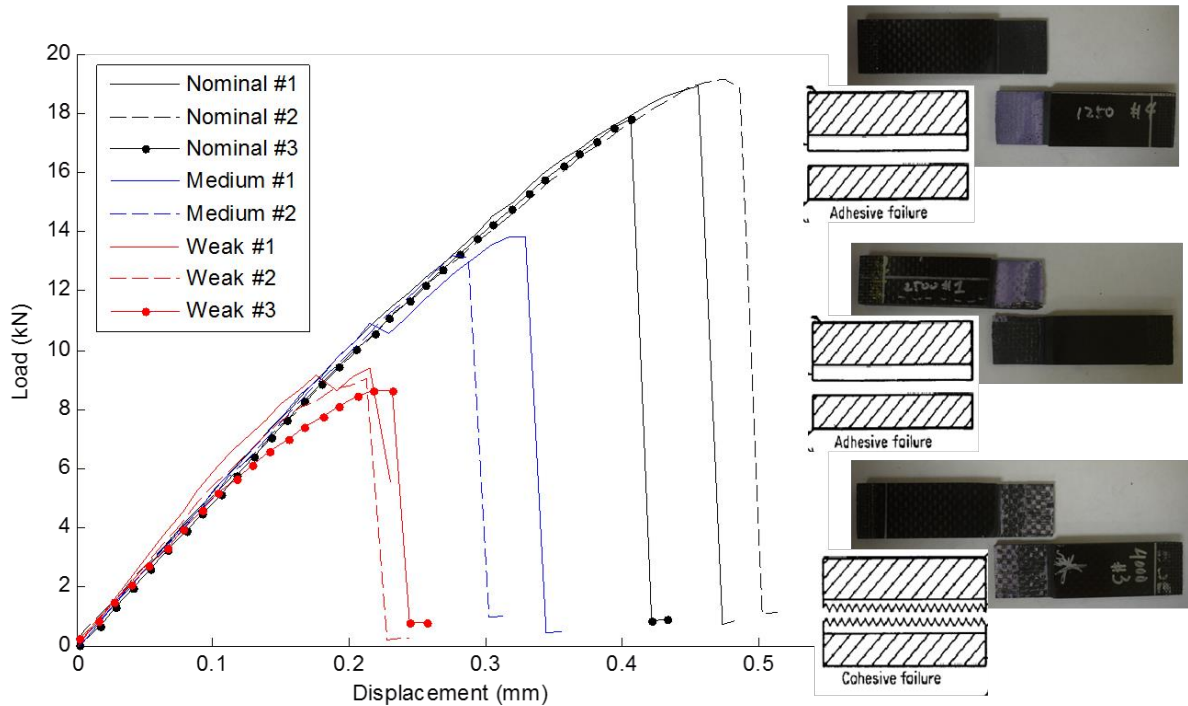


Figure 1: The load-displacement characteristic of bonded joints with three level of bondline strength and the failure pattern (top: weak; middle: medium; bottom: nominal).

2.2 Adhesively Bonded Aluminum Single Lap Shear Coupons

In this section we present the development of a process to prepare the adhesively bonded aluminum single lap shear coupons with commercially available PZT sensors (1/8 inch diameter) embedded in the bondlines. After their fabrication, the coupons were loaded under static loading to study the response of the embedded sensors. Single lap joints with PZT sensors embedded were prepared to investigate the relationship between the electromechanical impedance behavior of the sensors and the load history on the lap joints (see Figure 2 and

Figure 4). The samples were prepared following the ASTM D1002 (Standard Test Method for Apparent Shear Strength of Single-Lap-Joint Adhesively Bonded Metal Specimens by Tension Loading (Metal-to-Metal)), with 25.4 mm by 25.4 mm (1 inch by 1 inch) of bondline area for one sensor embedded.

Hysol EA 9696 adhesive film provided by Henkel was used to bond two aluminum alloy laps (2024 T5). Hysol EA 9696 is a modified epoxy film designed for applications requiring high toughness including aeronautics. The adhesive of this study was provided by John C. Osborne from Boeing Company. The adhesive films are sealed and stored in the -18 °C freezer in Structures and Composites Lab at Stanford. The surface preparation procedure is designed to follow the ASTM standard D2651, Standard Guide for Preparation of Metal Surfaces for Adhesive Bonding. The detailed preparation procedure is as follows:

- DI water rinse

- Abrade surfaces with sandpaper (3M Medium 100 Grit)
- Compressed air blow
- DI water rinse
- IPA rinse, rubbed with cotton
- DI water rinse
- Acetone rinse, rubbed with cotton
- DI water rinse
- Dried in 60 °C oven

In order to simulate the “kissing” bond behavior, different types of chemicals were used to degrade the bondline strength, including Teflon and graphite powder, two common materials found in manufacturing of carbon composite fibers. The result is shown in Figure 3. Graphite powder was used as the surface contaminate in the latter test due to its large influence on the bond strength and relative ease to handle.

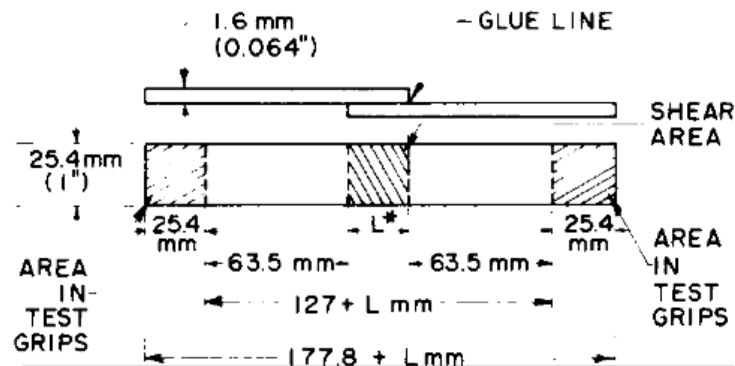


Figure 2: Suggested form and dimensions of test specimen from the ASTM D1002.

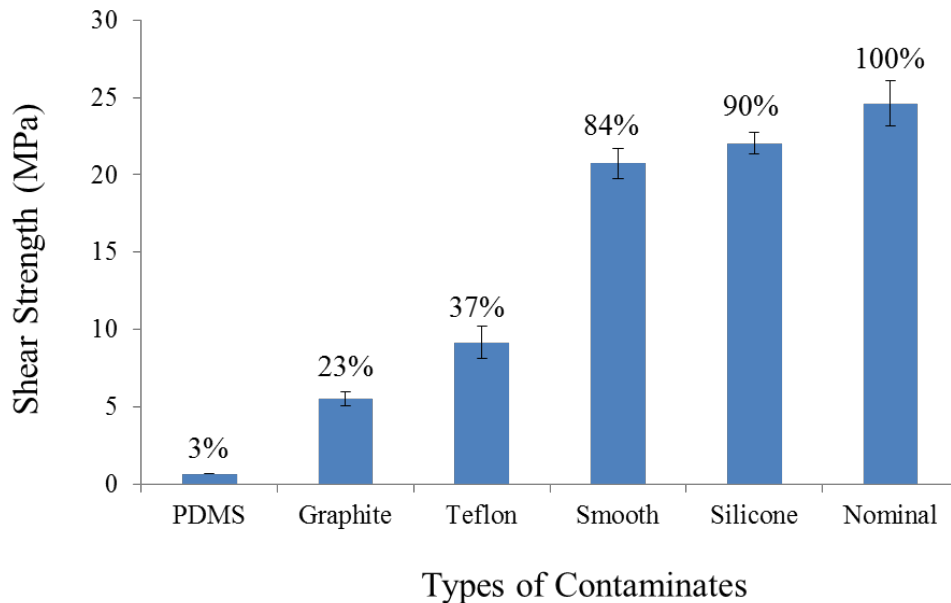


Figure 3: The influence of different surface contaminates on lap joint strength.

Piezoelectric disc sensors fabricated by APC ceramics were embedded into the bondline. The piezo material was Navy II type equivalent with 250 μm in thickness and 1/8 inch in diameter. The material properties can be found in Table 1.

Table 1: The properties of the piezoelectric material in APC disc sensor.

Density	Young's Modulus E_{11}	Young's Modulus E_{33}	Relative Dielectric Constant K_T	Piezo Charge Constant d_{33}	Piezo Voltage Constant g_{33}
7.6 g/cm^3	63 GPa	54 GPa	1900	400 pC/N	24.8 $\text{mV}\cdot\text{m}/\text{N}$

Due to the thickness of the piezoelectric disc sensors, three to four layers of adhesive film were used to fully encapsulate the sensors. Two varnished wires with diameter less than 100 μm were also embedded to extend the two electrodes of the sensor to the outside of the bondline, which are subsequently connected to an impedance analyzer. The lay-up of the sample is illustrated in Figure 4. Following the instruction of the manufacturer, the samples were cured under vacuum for 90 minutes at 121 $^\circ\text{C}$.

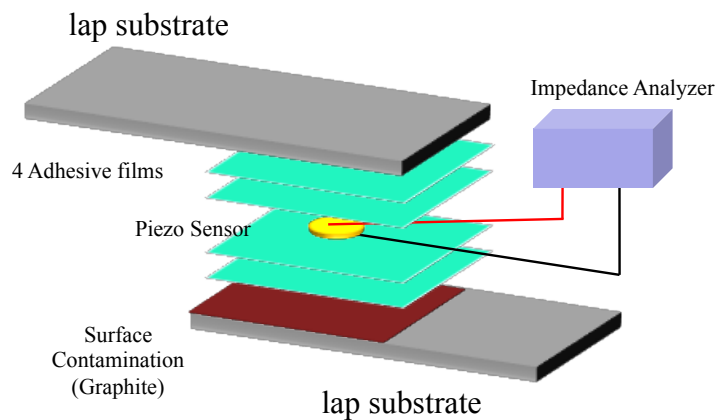


Figure 4: Illustration of a single lap joint with one piezoelectric sensor embedded in the adhesive bondline interface.

3. RESULTS

3.1 Impedance Behavior of Embedded Piezo-electric Sensors under Static Loading

The sample was loaded on a MTS (Material Testing System) so that the introduced cyclic load could further degrade the bondline integrity. The overall setup is shown in

Figure 5. The implemented cyclic load had an increasing peak load of 25 pounds step until sample failure and the impedance was measured under zero-loading condition by a SinePhase Z-check 16777k impedance analyzer. The impedance behavior of the piezo was recorded from 1 kHz to 2.5 MHz with an increment of 2 kHz. Both the real and imaginary impedance data were acquired.

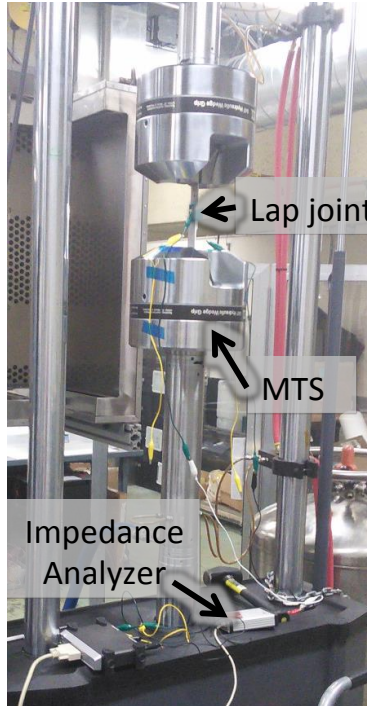


Figure 5: The experimental test setup.

Table 2: A total of 16 specimens, 8 nominal samples without contaminate and 8 with contaminates

	Nominal	Weak	Total
Batch 5	2	2	4
Batch 6	2	2	4
Batch 7	2	2	4
Batch 8	2	2	4
Total	8	8	16

A total of 16 samples were tested. The cyclic load with an incremental peak value was exerted on the specimens. A typical load history curve is as illustrated in Figure 1Figure 6.

After each load cycle, the electromechanical impedance was measured using the impedance analyzer. The typical impedance behavior of the samples is similar to Figure 7. There are two resonate peaks of impedance shown in the measured frequency bandwidth between 500 kHz to 2.5 MHz. The first peak is recorded around 800 kHz and the second peak with lower amplitude is found around 1.7 MHz. The similar impedance behavior was observed throughout all the samples under all loading conditions with slightly differences in the frequency and amplitude.

We investigated several existing literature damage indices to evaluate the influence of the load cycle on the behavior of the piezoelectric sensors and the bondline integrity. We selected the root mean square deviation (RMSD) as the appropriate damage index, which described the averaged impedance change from the baseline sample without any loading. The definition of RMSD is

shown below, where $Z_h(\omega_i)$ is the healthy bond's impedance, $Z_i(\omega_i)$ is the unknown or damaged bond's impedance and ω_i is the frequency interval.

$$\sqrt{\frac{\sum_{i=1}^n [Re(Z_h(\omega_i)) - Re(Z_u(\omega_i))]^2}{\sum_{i=1}^n [Re(Z_h(\omega_i))]^2}}$$

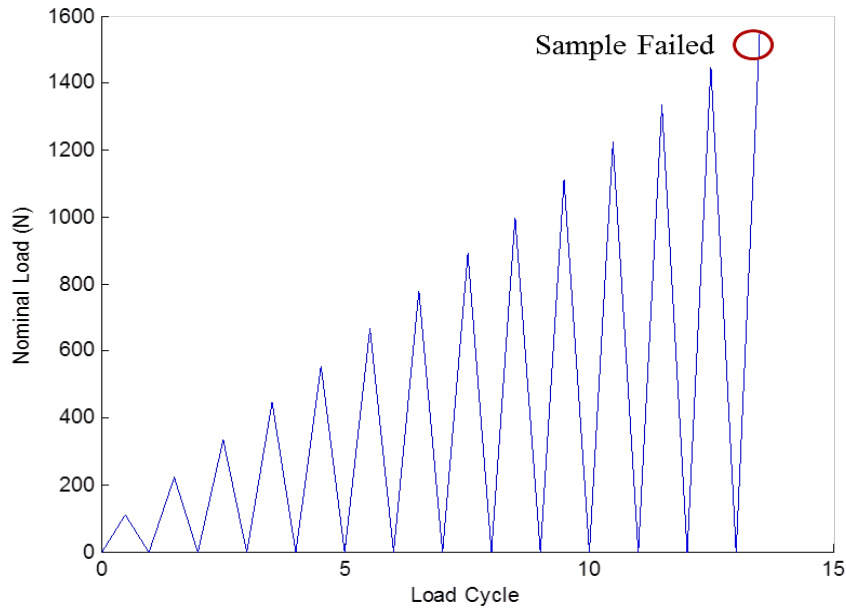


Figure 6: Typical load cycle with the impedance measured under the unloaded condition.

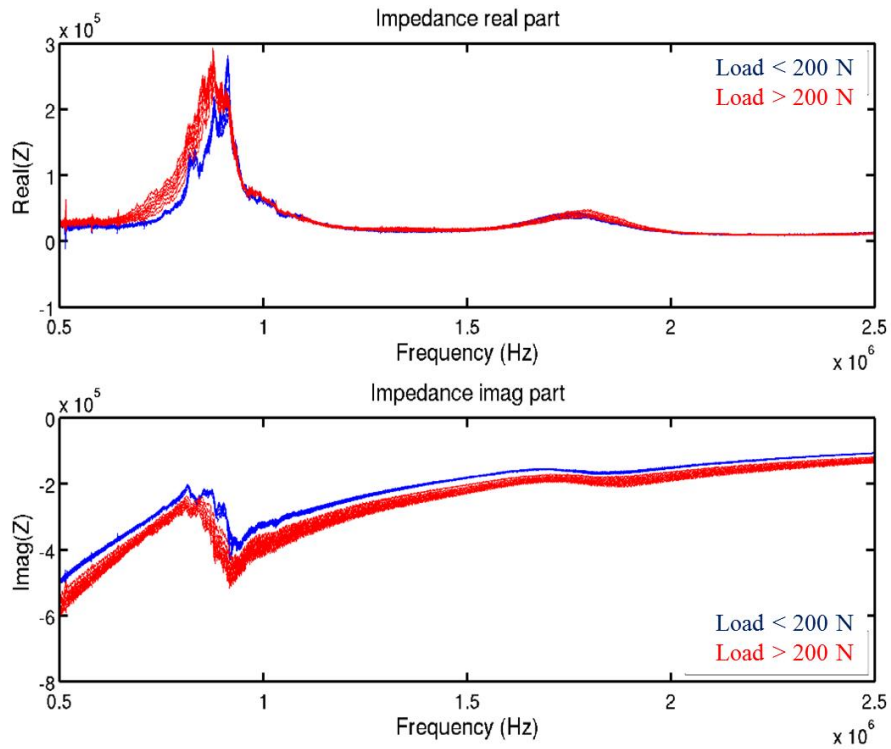


Figure 7: Typical electro mechanical impedance behaviour obtained from experimental samples.

We estimated the damage index around the first peak frequency and within a range of 100 kHz. Regardless of the existence of surface contaminates, all samples showed a similar behavior, i.e. the damage index was relatively constant until the sample was exposed to a certain level of load cycle and approaching failure. It implied that by measuring the impedance and the deviation of impedance from the intrinsic sample, it is possible to predict the failure of the bonded joint and estimate the degradation of the bondline. For example, as shown in Figure 8, we chose the 2% damage index as an arbitrary threshold to characterize the bondline state as healthy or degraded.

Since the strength of the bondline was different across different batches, the max stress in load cycles was normalized by the strength of the bondline. The results are shown in Figure 9. It is evident that all the curves, except B6N2, show the same trend, i.e. the damage index stays relatively constant regardless of the stress experienced up until around 80% ~ 90% of the failure stress. After this stress threshold, the damage index increases dramatically with the corresponding increase of the load, which implies that the failure is approaching. The curves of B6N2 showed a similar trend while the damage index ramped up after a much lower stress level. After the test, we observed that the sensor was fractured, which hadn't been seen on other samples, and it indicated that the outlier was due to the premature failure of the embedded sensor.

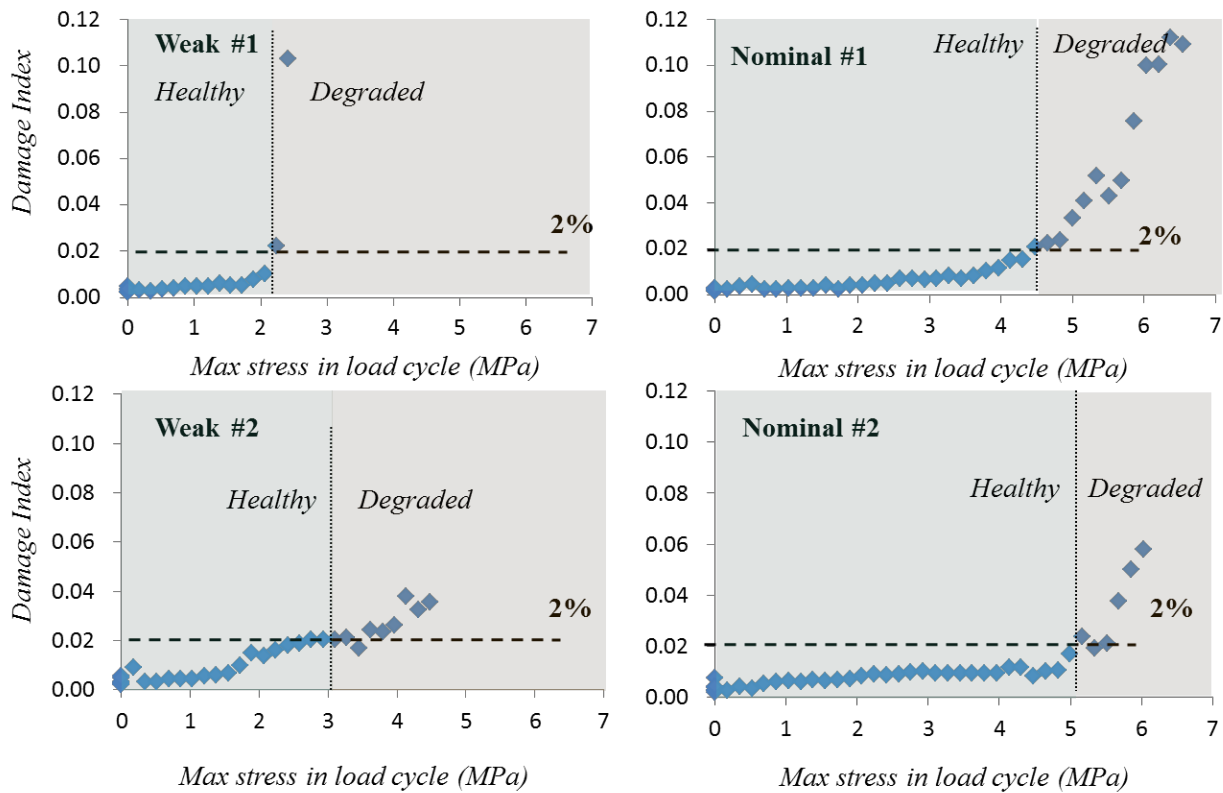


Figure 8: The damage index (root mean square deviation) of both weak and nominal samples exhibited a similar trend.

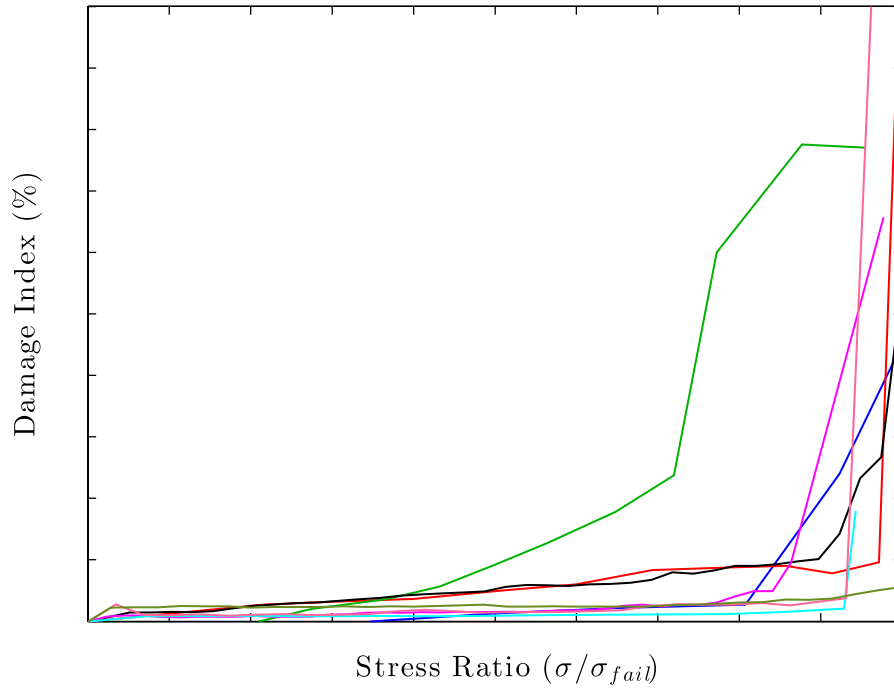


Figure 9: The damage index (root mean square deviation) of most samples exhibited a similar trend: a large increase of the index after 80% to 90% of the lap joint strength.

3.2 Finite Element Simulation Study

The finite element model (FEM) has been developed using the commercial software Abaqus 6.12 to simulate the impedance behavior of the embedded sensors in the bondlines. The aim was to obtain an accurate result of the impedance behavior over the large frequency bandwidth using the direct steady-state linear dynamic analysis. The element of C3D8E was used as the piezoelectric element and the mesh had a typical dimension of 100 μm to capture all the motion and deformation of the sensor.

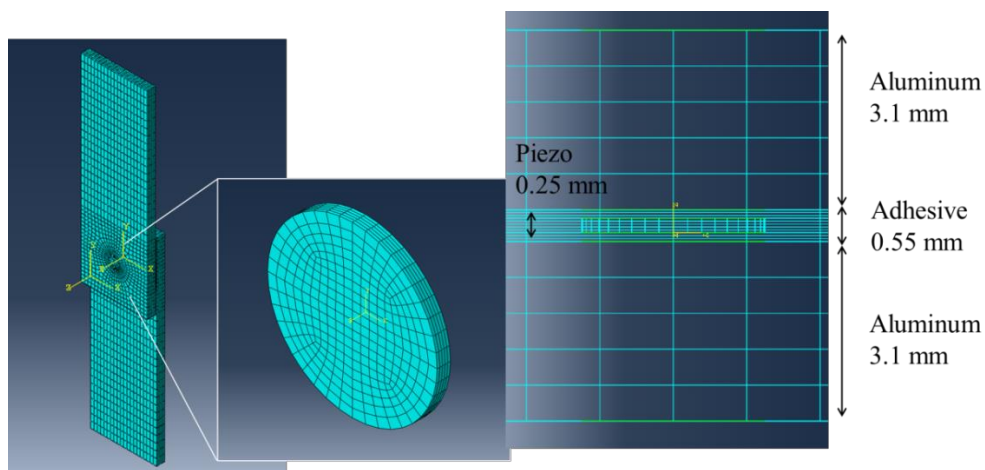


Figure 10: The FEM model and mesh of the bondline with embedded piezo sensor disc.

The material properties used in the simulations are shown in the following tables.

Table 3: Material properties used in the numerical simulations.

Property	Unit	Aluminum Al 2024-T3	CFRP T800S/3900-2	Adhesive Hysol®EA 9696	Piezo PZT-5A
E_{11}	GPa	69.00	156.00	2.60	60.97
E_{22}	GPa	69.00	9.09	2.60	60.97
E_{33}	GPa	69.00	9.09	2.60	53.19
G_{23}	GPa	25.94	3.24	1.00	21.05
G_{31}	GPa	25.94	6.96	1.00	21.05
G_{12}	GPa	25.94	6.96	1.00	22.57
ν_{23}		0.33	0.400	0.30	0.4402
ν_{13}		0.33	0.228	0.30	0.4402
ν_{12}		0.33	0.228	0.30	0.3500
ρ	kg m ⁻³	2700	1540	1100	7750

$$\mathbf{d} = \begin{bmatrix} 0 & 0 & 0 & 0 & 584 & 0 \\ 0 & 0 & 0 & 584 & 0 & 0 \\ -171 & -171 & 374 & 0 & 0 & 0 \end{bmatrix} \times 10^{-12} \text{ C N}^{-1} \quad \boldsymbol{\varepsilon}_\sigma = \begin{bmatrix} 1730 & 0 & 0 \\ 0 & 1730 & 0 \\ 0 & 0 & 1700 \end{bmatrix} \times \varepsilon_0$$

The impedance behavior from 50 kHz to 2 MHz was determined at the interval of 5 kHz. The results of both real and imaginary parts are illustrated in **Error! Reference source not found.** in blue color. The corresponding experimental results are shown in red color. Without any further calibration of the material properties as well as the dimension of the bondline, the simulation matched the experimental result to a certain extent in both the frequency and amplitude.

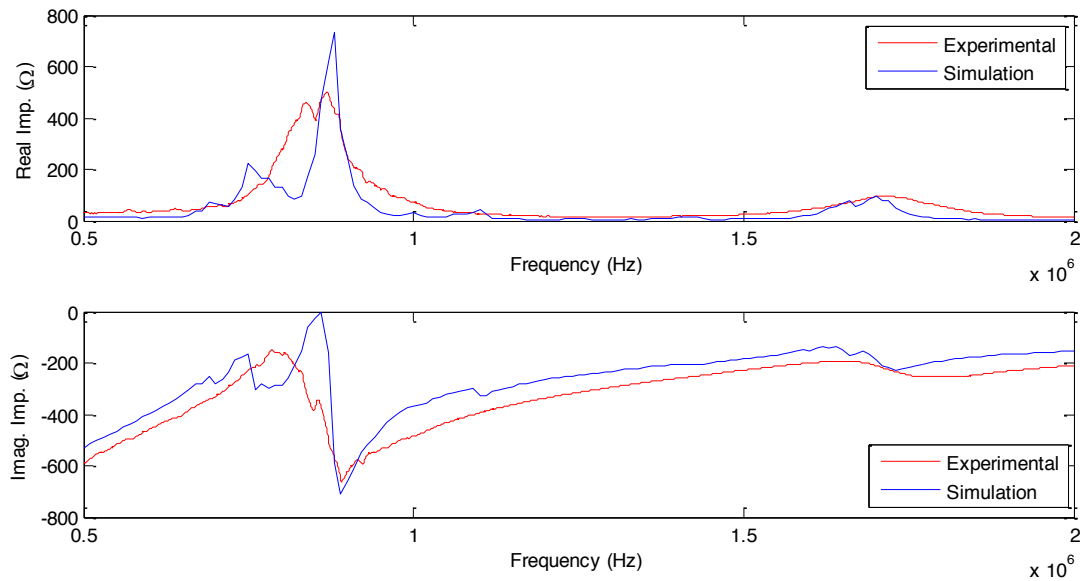


Figure 11: Comparison of numerically simulated and experimentally obtained impedance behaviour for a piezoelectric sensor embedded in the adhesive bondline.

In the literature, it was recommended that the kissing bond could be modeled by decreasing the stiffness of the interfacial element between adhesive and adherent [2,3]. The typical thickness of the element is 10 μm . The stiffness of the interfacial element is tuned to different levels to simulate the severity of the bondline degradation due to kissing bond as shown in Figure 12.

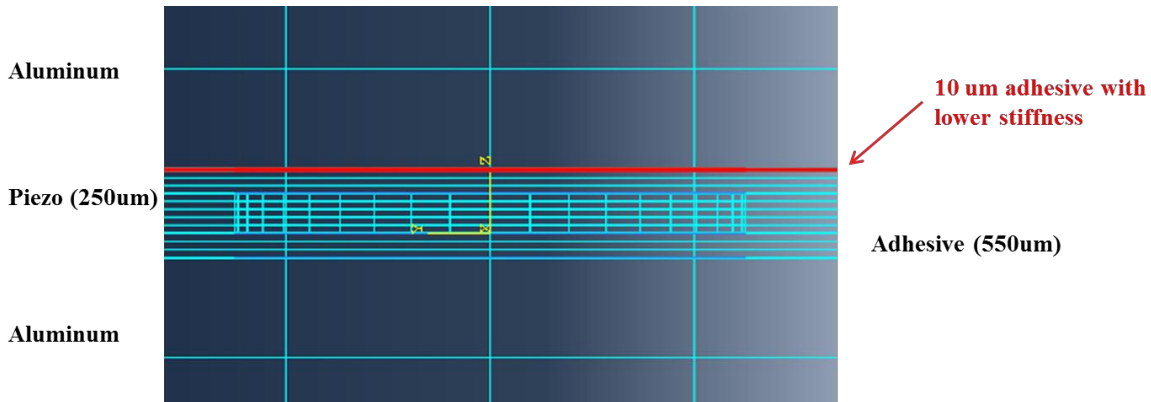


Figure 12: Kissing bond simulation is achieved via the reduction of the stiffness of the interfacial elements.

The effects of decreasing the interfacial elements' stiffness on global stiffness of the structure was also studied. 1967 pounds (8750 N) force was applied on one end of the single lap while the other end was fixed. The resultant displacement was 6.4×10^{-3} inch (0.163 mm) for the model when no interfacial elements' stiffness was decreased, and 6.5×10^{-3} inch (0.165 mm) for the model when the interfacial elements' stiffness was decreased to 10% of the original stiffness. The decrease of interfacial elements' stiffness by 90% led to 1.4% increase of the end displacement. In conclusion, the global stiffness is insensitive to the interfacial element stiffness, which was confirmed by the experiments and shown in Figure 1. The stiffness was lowered from 10% to 90% and the result of simulation was plotted in Figure 13. With the decrease of the stiffness, the peak of impedance first decreases in the amplitude. After certain level, the peak of impedance starts to increase while the frequency of the peak decreases. The similar trend was observed experimentally when the load level of the sample increased and the damage level of the bondline became more severe as shown in Figure 14.

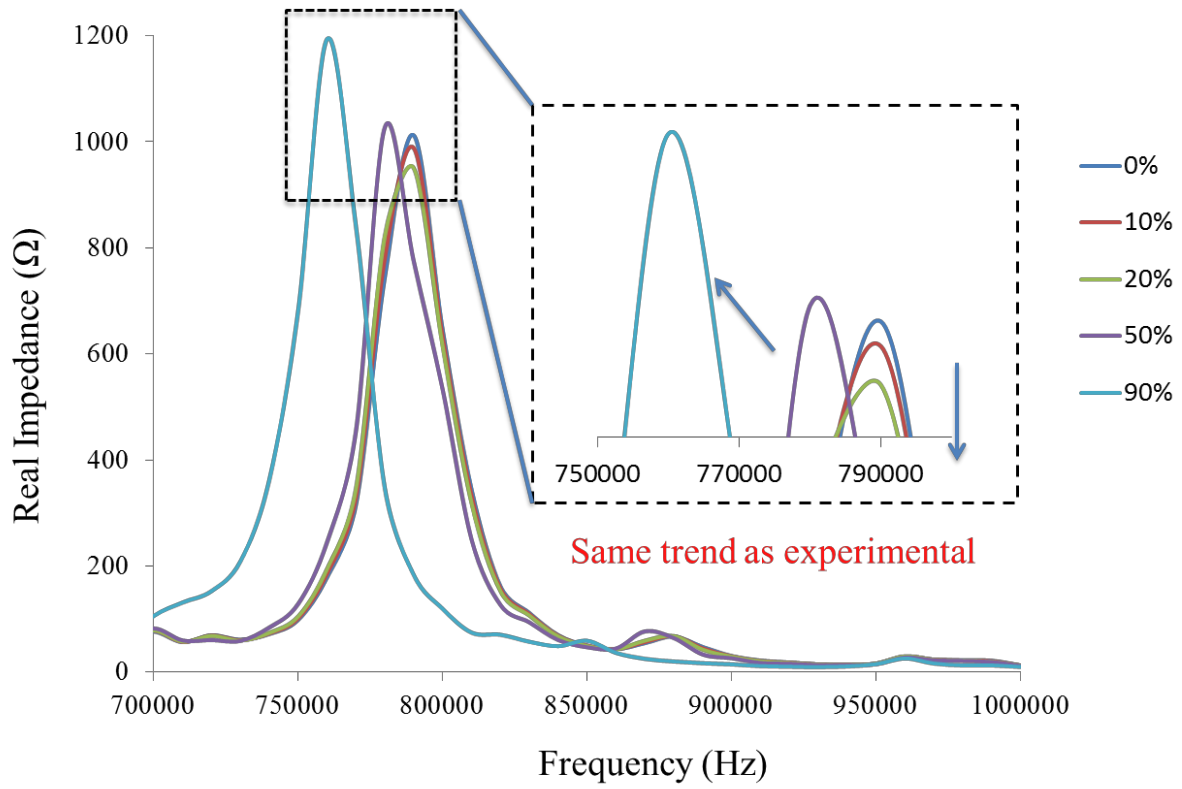


Figure 13: Numerical results for the simulation of the bondline integrity degradation due to kissing bond.

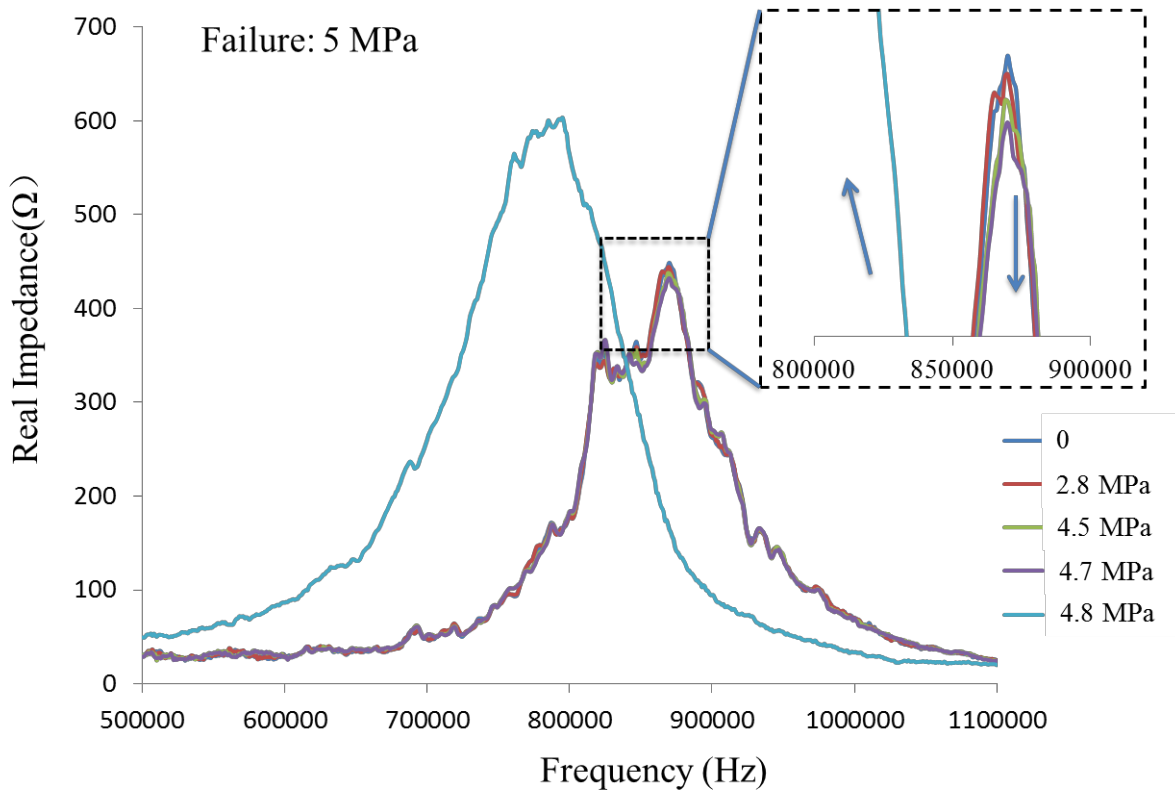


Figure 14: Experimental results of the impedance show a similar trend as the simulation results.

4. CONCLUSIONS

Compared to conventional bolted joints, bonded joints have superior mechanical properties in terms of light weight, less stress concentration etc. However, due to the lack of confidence on the bondline integrity level during fabrication and service, the large adaption of bonded joints onto airplane primary structural components is restricted by regulations and standards. Among all the defects that can be found in adhesive bondlines, one type of interfacial weakness, the kissing bond, is the most challenging one. This is due to the catastrophic failure it can cause to the bondline as well as to the almost impossible early detection using conventional non-destructive evaluation (NDE) or structural health monitoring (SHM) techniques. From the samples of bonded carbon fiber reinforced plastic panels with simulated kissing bond fabricated by Boeing, a loss of more than 50% strength was observed without any significant change on global stiffness. In order to reproduce the kissing bond in our laboratory setting, several types of chemicals were tested to contaminate the interface between adhesive and adherent in the aluminum single lap joint. Graphite was chosen to reproduce kissing bond for the future study.

With the capability to simulate kissing bond behavior, we developed and tested a break-through technique to monitor the bondline integrity by embedding piezoelectric sensors into the bonded joints. The impedance-based detection algorithms were used by measuring the electromechanical impedance of the embedded sensors. Since the sensors are positioned in the bondlines, close to the interface of adhesive and adherent, where the kissing bond could occur, any small change in the interface would affect the EMI response of the sensor. The EMI behavior of the embedded sensor under static loading was studied. The single lap joints with sensor embedded inside were exposed to an incremental tensile load. The impedance was recorded under zero load condition before a higher load was exerted on the sample. Across all the tested samples, a similar behavior was observed, i.e. the impedance of the sensor is kept constant until a certain load level, after which, the impedance changes dramatically from the pristine state. The root mean square deviation was defined as the damage index to quantify the change of impedance.

A finite element model was also developed to investigate the impedance behavior of the embedded piezo sensor. In order to simulate the behavior of kissing bond, the stiffness of the interface elements of the adhesive was degraded. The degradation of this 10 μm thick element would not affect the global stiffness of the lap joint, however, it would affect the impedance behavior of the embedded sensors significantly. Preliminary simulation results matched with the experimental result qualitatively and similar trend of the decrease of resonate frequency was seen when the sample was prone to failure.

Future work will include the study of the effect of the sensors' locations in the bondlines in order to improve the detectability; to validate the impedance-based algorithms under dynamic and fatigue loading; and the development of piezo-electric sensors with smaller dimension so that much less parasitic effect would be introduced when the sensor was embedded in the bondlines. An innovative piezo-electric ceramic sensors are being developed at Stanford via screen-printed techniques. The screen-printed electric ceramic piezo-sensors can provide the needed EMI performance for the impedance-based algorithms for bondline integrity monitoring and meet the thickness requirements (typically 20~30 μm) for bondlines application.

5. REFERENCES

1. C.J. Brotherhood, B.W. Drinkwater and S. Dixon, "The detectability of kissing bonds in adhesive joints using ultrasonic techniques", *Ultrasonic*, Volume 41, Issue 7, Sept 2003, pp 521-529
2. G.M. Light and H. Kwun, "Nondestructive Evaluation of Adhesive Bond Quality, State-of-the-Art Review", NTIAC-89-1, 1989.
3. D. Jiao and J.L Rose, "An Ultrasonic Interface Layer Model for Bond Evaluation", *J. Adhesion Science and Technology*,5, 631(1991).
4. P.B. Nagy, "Ultrasonic classification of imperfect interfaces", *J. Adhesion Science and Technology*, 5, pp.619-630(1991).
5. A. Baltazar, S.I. Rokhlin, C. Pecorari, "The relationship between ultrasonic and micromechanical properties of contacting rough surfaces", *J. Mech. Phys. Solids*, 50 (2002), pp. 1397-1416
6. J.B. Ihn and F.K. Chang, "Built-in diagnostics for monitoring crack growth in aircraft structures", *Proceedings of the 3rd international Workshop on Structural Health Monitoring*, Stanford, CA, pp. 284-295, Sept 2001.
7. J.B. Ihn and F.K. Chang. 2004, "Hot spot monitoring for aircraft structures", *Advanced Smart Materials and Smart Structures Technology*.
8. J.B. Ihn and F.K. Chang. 2004, "Detection and monitoring of hidden fatigue crack growth using a built-in piezoelectric sensor/actuator network", *Smart Material Structure*, 13,609-620
9. J.D. Achenbach, O.K. Parikh, "Ultrasonic analysis of nonlinear response and strength of adhesive bonds", *J. Adhes. Sci.*,5 (8)(1991), pp 601-608.
10. Z. Tang, A. Cheng, J.D. Achenbach, "An ultrasonic technique to detect nonlinear behaviour related to degradation of adhesive joints", in: D.O. Thompson, D.E. Chimenti (Eds.), *QNDE*, vol. 17, Plenum Press, New York, 1998.
11. N. Wang, O. I. Lobkis, S. I. Rokhlin, and J. H. Cantrell, "Ultrasonic characterization of interfaces in composite bonds", *AIP Conf. Proc.*, 1335, 1079 (2011)
12. A. Baltazar, L. Wang, B. Xie, and S.I. Rokhlin, "Inverse ultrasonic determination of imperfect interfaces and bulk properties of a layer between two solids", *Acoustical Society of America.*, 114 (3)(2003), pp1424-1434.
13. S.I. Rokhlin, L. Wang, B. Xie, V.A. Yakovlev, L. Adler, "Modulated angle beam ultrasonic spectroscopy for evaluation of imperfect interfaces and adhesive bonds", *Ultrasonic*, 42 (2004), pp. 1037-1047.
14. S.I. Rokhlin, B. Xie and A. Baltazar, "Quantitative ultrasonic characterization of environmental degradation of adhesive bonds", *J. Adhesion Sci. Technol.*, Vol. 18, No. 3, pp. 327-359 (2004)
15. B. Eehart, B. Valeskes, C.E. Muller, C. Bockenheimer, "Methods for the Quality Assessment of Adhesive Bonded CFRP Structures -A Resumé", 2nd International Symposium on NDT in Aerospace 2010, We.5.B.2
16. F.J. Margetan, R.B. Thompson, and T.A. Gray, "Interfacial Spring Model for Ultrasonic Interactions with Imperfect Interfaces: Theory of Oblique Incidence and Application to Diffusion-Bonded Butt Joints", *Journal of Nondestructive Evaluation*, Vol 7, Nos. 3/4,1988
17. E. Maeva, I. Severina, S. Bondarenko, G. Chapman, B. O'Neil, F. Severin, and R. Gr. Maev, "Acoustical methods for the investigation of adhesively bonded structures: A review", *Can. J. Phys.*,82: 981-1025 (2004).